Particle tracking during melting and solidification in the presence of AC magnetic field of various configurations

V Bojarevics, K Pericleous

Particle tracking during melting and solidification in the presence of AC magnetic field of various configurations

V. Bojarevics and K. Pericleous

University of Greenwich, London SE10 9LS, UK

Corresponding author: v.bojarevics@gre.ac.uk

Abstract
The AC electromagnetic field effects in molten metal are investigated to account for the mixing of particles (grain refiners, micro/nano additives, impurities, broken metal dendrite agglomerates, bubbles) during the full melting/solidification cycle. The particles travel due to the hydrodynamic drag, buoyancy, turbulent fluctuations and the electromagnetic force action via the local pressure distribution around the particle. The time average effects are investigated previously using approximation derived for a uniform electric and magnetic fields. In the presence of AC field the force distribution is non-uniform, confined to an exponential skin-layer near the outer surface of liquid. This typically results in high mixing rates and an intense turbulence in the bulk of molten metal, additionally contributing to the particle dispersion. The paper attempts to demonstrate the importance of each of the mentioned effects to the organized particle 'swarm' like transport and the eventual distribution. Three different examples of the mixing flows generated by AC fields are presented: a travelling field stirring during directional solidification, the semi-levitation dynamic melting and the contactless top coil 'immersion' mixing involving the dynamic AC field adjustment. The Lagrangian particle tracking in the presence of strong AC electromagnetic force field gives new perspectives to the understanding of the melting and casting processes.
Key words: particle tracking, electromagnetic mixing, melting, solidification

Introduction

Aluminium, magnesium and titanium alloys are the light structural metals attractive for aerospace and automotive applications. Research efforts are aimed at developing new casting techniques and practices to ease inherent processing difficulties of these alloys to achieve more desirable mechanical properties for critical automotive structural and kinetic components. One major barrier to casting these components is melting and subsequently casting homogeneous alloys free of contamination and severe segregation, or alternatively adding uniformly dispersed micro to nano particles to create a composite alloy of enhanced mechanical properties. A finer microstructure usually improves the mechanical properties of the solidified alloy. Finer microstructure can be achieved by increasing the cooling rate, adding dispersed micro to nano size particles of other materials or distributing broken dendrite fragments of the same material as grain refiners. The additional stirring eases the restrictions on the cooling rate during the casting process. It is well known that forced stirring of the melt by electromagnetic forces can significantly promote the detachment of dendrite arms and transporting the crystal fragments in a disperse fashion due to the presence of high turbulence [1]. However, unidirectional stirring in laminar conditions could induce undesirable channel segregation in the solidifying material [2]. Therefore the electromagnetic stirring [3] must be applied in an optimized way designed for a particular process.

The large scale electromagnetically driven flow circulation exerts a drag force which contributes to the particle transport. The particles travel due to the hydrodynamic drag, buoyancy, turbulent fluctuations [4] and the electromagnetic force action via the local pressure distribution around the particle. A significant contribution to the force balance arises from the so called electro-magnetophoretic forces [5], which are well known for a variety of MHD applications, such as removal of inclusions from steel melt [6,7], concentrating electrically insulating bubbles [8,9] or insulating particles collected near the surface [10], and for many other purposes of separation or mixing [11]. The electromagnetic force acts directly onto electrically conducting inclusions, however the electromagnetic force in the surrounding fluid creates the pressure distribution gradient leading to the integral force on the non-conducting inclusions. Often the electromagnetic force expression is used as derived by Leenov & Kolin [5] in the case of particles positioned in a constant crossed electric and magnetic fields. Experimental observations of the particles of various shapes and electrical conductivities in the liquid metal carrying electrical current are described in [12], where the expression similar to Leenov, Kolin's was derived, but for the conditions of gradient magnetic field, which results in the increase of the effective force on the particles. In the AC magnetic field the time average force effects are often treated using the same formulae as for the constant uniform fields. The latter contradicts the skin-layer distribution of the exponential force distribution in the AC field [13]. Moreover, the total force in AC field contains also the pulsating part contributing to the particle drag by the 'history' and 'added mass' contributions. The high mixing rates ensure the intense turbulence in the bulk of molten metal, additionally affecting the particle dispersion. This paper attempts to demonstrate the importance of each of the mentioned effects to the organized particle 'swarm' like transport and the

eventual distribution when the melt solidifies to final ingot of modified impurity distribution. The pseudo-spectral numerical method is extended to account for the presence of particles during the melting/mixing/solidification cycle in presence of single and multiphase AC magnetic fields. Three different examples of the mixing flows generated by AC fields are presented: a travelling field stirring during directional solidification, the semi-levitation dynamic melting and the contactless top coil 'immersion' mixing involving the transient AC field adjustment.

Mathematical modelling

The mathematical modelling of the complex time dependent problem describing initially a solid body heating, the melting process and subsequent liquid metal confinement dynamics, internal fluid flow and the temperature evolution is accomplished using the SPHINX code developed at the University of Greenwich [14,15]. While in the temperature limit below melting the solid body heating is solved in the continuously adjusted electromagnetic field from the (possibly moving) source coils. The time dependent Joule heating eventually leads to melting of the solid. When the solidus temperature is reached, the model accounts for the phase transition and the following liquid material shape change due to the action of the EM force distribution adjusted to the moving interface. The fluid flow is solved using the Reynolds averaged turbulent flow model for an incompressible fluid with the effective viscosity ν_e and the turbulent diffusivity α_e modified heat transfer equations given in detail elsewhere [14,15]. The boundary conditions are prescribed dynamically on the moving liquid interface. The free surface boundary conditions are determined by the tangential and normal stress components accounting for the temperature dependent surface tension $\gamma(T)$. The method is based on the continuous co-ordinate transformation adapting to the free surface and the containing vessel shape. The present implementation adds the Lagrangian passive particle tracking algorithm. The position **R**(x,y,z,t) of an individual particle can be determined following its path and the variable total force **F**(x,y,z,t) acting on the particle by solving the set of two equations [4,16]:

$$\partial_t \mathbf{R} = \mathbf{u}_p, \qquad m_p \partial_t \mathbf{u}_p = \mathbf{F}, \tag{1), (2}$$

where $\mathbf{u}_p$ is the particle velocity and m_p its mass. The force **F** acting locally on the spherical particle can be decomposed into the fluid drag force $\mathbf{F}_d$, the buoyancy force $\mathbf{F}_g$ and the effective electromagnetic force $\mathbf{F}_e$. The drag force depends on the Reynolds number $Re_p = r_p |\Delta \mathbf{u}| / \nu$, where r_p is the particle radius, $\Delta\mathbf{u} = \mathbf{u} - \mathbf{u}_p$ is the (slip) velocity relative to the fluid velocity **u**, ν – the kinematic viscosity. For small particles (1nm -100 μm) the Reynolds number Re_p is rather small, of the order 0.1 - 10, therefore the drag force can be approximated as instantaneous modified Stokes formula [16]. The buoyancy force due to the gravity **g** action on the particle and the surrounding fluid is $\mathbf{F}_g = (\rho_p - \rho) V_p \mathbf{g}$, ρ is the fluid density, ρ_p – the particle density, V_p – the particle volume. The electromagnetic force acts on the induced electric current in the particle [3] and due to the fluid pressure redistribution on the surface of the particle. For the case of electrically non-conducting particles (oxides, carbides, dendrite fragments, bubbles etc.) the electromagnetic force in the AC skin-layer can be derived as $\mathbf{F}_e = -V_p (\frac{3}{2} \widehat{\mathbf{f}}_e + \mathbf{f}'(t))$, the sum of the time average and the oscillating components in the fluid at the location of the particle. Note, the Leenov, Kolin [5] expression derived for DC constant fields $\mathbf{F}_{eDC} = -V_p \frac{3}{4} \mathbf{f}_e$ gives two times smaller force acting on a non-conducting particle. The presence of the oscillating force component requires the modified drag expression for an oscillating spherical particle [17]:

$$\mathbf{F}_d = 6\pi\nu\rho r_p [(1+\varepsilon)\Delta\mathbf{u} + \frac{\varepsilon}{\omega}(1+\frac{2}{9}\varepsilon)\frac{d\Delta\mathbf{u}}{dt}], \qquad \varepsilon = \sqrt{\frac{\omega r_p^2}{2\nu}}, \tag{3}$$

where the Stokes number ε can reach an order 1 in an AC field oscillating at typical frequencies $\omega \sim 10^3$ - 10^4 Hz. The equation (3) contains the instantaneous Stokes drag, the memory term (Basset force) and the added mass force.

The typical mixing flow is turbulent ($Re \sim 10^3$ - 10^4), which further requires a modification due to the stochastic part of velocity in accordance to the resolved turbulent kinetic energy k and the local eddy life time (or the particle transit time in that eddy, whichever is the shortest) [4]. The use of k- ω turbulence model in the SPHINX code facilitates to obtain these quantities, which are locally interpolated to the particle position at each time step. The numerical integration of equations (1) and (2) is done for each individual particle of various properties depending on the initial seeding locations. The time dependent forces **F** are sensitive to the location and the instantaneous update of local slip velocity $\Delta\mathbf{u}$ (including the stochastic contribution). Therefore, the stability of long term integration along the particle tracks can be adversely affected by the choice of numerical integration scheme. The classical explicit integration schemes are limited to extremely small time steps, which could make the numerical solution difficult for the dynamic flow conditions. The exponential numerical scheme, proposed in [15], permits stable time integration of the particle tracks with the time steps of the order 0.1 - 1ms (adjustable) used for the unsteady fluid flow solution in the examples considered below.

Numerical solution examples

In a typical induction melting crucible of cylindrical shape the coil is coaxially surrounding the liquid zone, for instance as in the Figs. 4,5. The computed force distribution is shown in the Fig. 1 comparing the 1 kHz and 11 kHz cases. The

relatively large particle of 1mm is shown in the skin-layer to demonstrate the steep force change over the size of particle. The full AC force variation in the Fig. 2 is computed for several AC periods using 100 time steps per period for the top coil immersed mixing application (see the Fig. 3). The force amplitude is very large under the top coil due to the extreme proximity effect achieved in this application [18]. This helps to produce a strong jet and the turbulent mixing required to disperse the particles initially added on the top surface, Fig. 3.

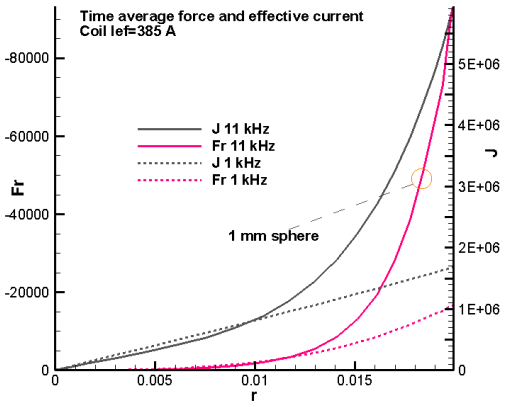

Fig. 1: Time average force and the electric current radial distribution in the cylindrical crucible, showing a small sphere for a scale comparison.

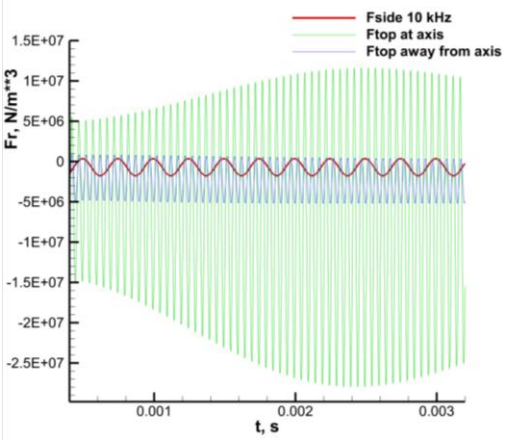

Fig. 2: Oscillating force distribution for the top coil (1700 A, 10 kHz) and the side coil (1600 A, 2 kHz) joint action.

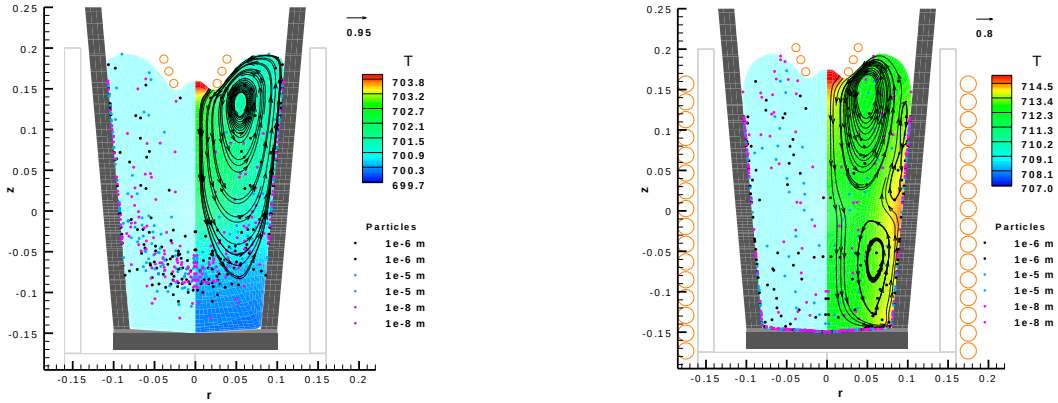

Fig. 3: Nano and micro particle cloud tracking for top coil metal matrix melt preparation device: (left) the top coil (10 kHz) and (right) the top and side coil (2 kHz) joint action.

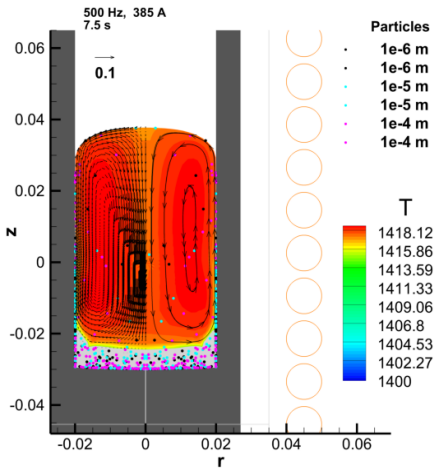

Fig. 4: The effect of upward travelling field at 500 Hz on particles in directionally solidified Si.

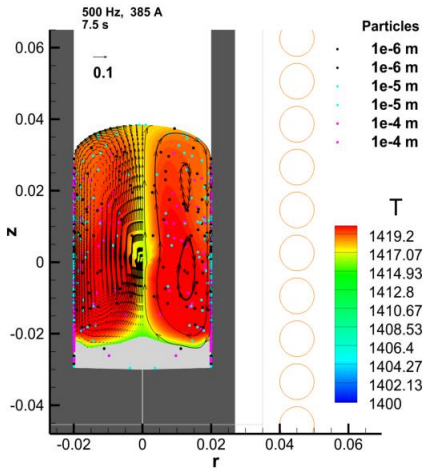

Fig. 5: The effect of downward travelling field at 500 Hz on particles in directionally solidified Si.

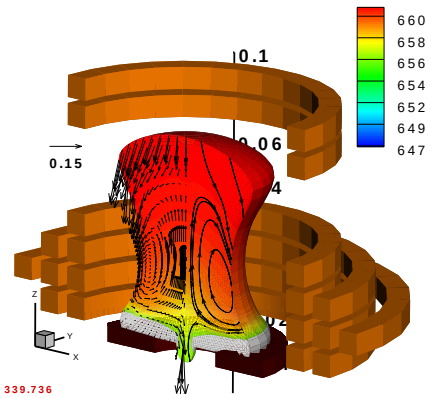

Fig. 6: Semi-levitation melting at the final stage when liquid pouring starts.

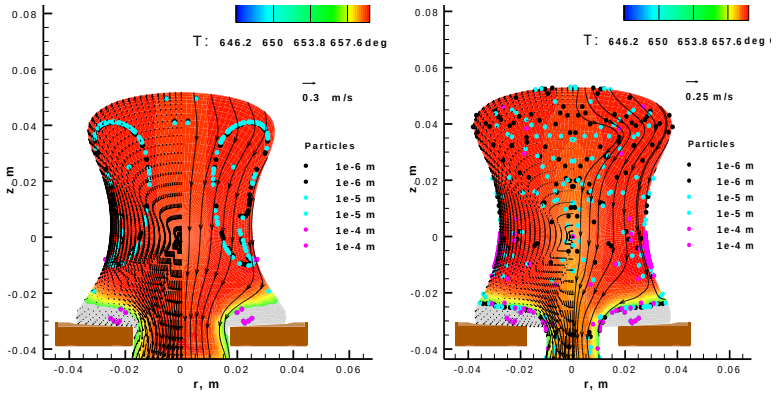

Fig. 7: The particle distribution without (left) and with (right) the oscillating and stochastic contributions.

The second example shows two different SiC particle distribution types achieved when using the travelling magnetic field type of mixing during the silicon material solidification. The upward travelling field produces fast engulfment of the particles in the bottom zone (Fig. 4), while the downward travelling field creates conditions to collect the particles at the side wall (Fig. 5), though at much slower rate. The third example is for a containerless semi-levitation melting process [19,14]. The electromagnetic field induces a strong turbulent flow in the molten pool, which is beneficial for producing a homogeneous melt with uniform temperature. The process combines induction melting and casting into a single self-controlling operation. The charge is melted from top to bottom through movement of the induction coil as illustrated in Fig. 6. Pouring of the charge through the hole in the chill block into the mold below occurs when the liquid melting front reaches the base of the metal charge. Fig. 7 compares the particle instantaneous positions after the random seeding in the initial solid cylinder, melting and mixing for 340 s, then pouring while the magnetic confinement and mixing is maintained. The mixing patterns in organized particle 'loops' are created when neglecting the turbulent fluctuations and the oscillating force, while the full AC force contribution creates more realistic particle distribution.

References

[1] T. Campanella, C. Charbon and M. Rappaz. Metall. Materials Transactions 35A (2004) 3201-3210.
[2] M. Medina, Y. Du Terrail, F. Durand, Y. Fautrelle. Metall. Materials Transactions 35B (2004) 743-754.
[3] H.K. Moffatt. Phys. Fluids, 3A (1991) 1336-1343.
[4] P.G. Tucker. Journ. Fluids Eng., 123 (2001) 372-381.
[5] D. Leenov and A. Kolin. Journ. Chem. Phys., 22, N 4 (1954) 683-688.
[6] T. Toh, H. Yamamura, H. Kondo, M. Wakoh, Sh. Shimasaki, S. Taniguchi. ISIJ International, 47, No 11 (2007) 1625-1632.
[7] L. Barnard, R.F. Brooks, P.N. Quested and K.C. Mills, Ironmaking and Steelmaking, 20, N 5 (1993) 344-349.
[8] J.W. Haverkort, T.W.J. Peeters. Metallurgical and Materials Transactions, 41B (2010) 1240-1246.
[9] V. Bojarevics, A. Roy. Magnetohydrodynamics, 48, N 1 (2012) 125-136.
[10] S. Taniguchi, A. Kikuchi. Proc. 3rd Int. Symp. Electromagn. Proc. Materials, ISIJ, Nagoya, (2000) 315-320.
[11] L.Zhang, Sh. Wang, A. Dong, J. Gao, L.N.W. Damoah. Metall. Materials Trans., 45B (2014) 2153-2185.
[12] V. Bojarevics, J. Freibergs, E. Shilova, E. Shcherbinin, Electrically Induced Vortical Flows, Kluwer Academic Publishers, Dordrecht, Boston, London, (1989).
[13] J. Etay (2009), private communication.
[14] V. Bojarevics, K. Pericleous and M. Cross. Metall. Materials Trans., 31B (2000) 179-189.
[15] V. Bojarevics, K. Pericleous and R. Brooks. Metall.Materials Trans., 40B, N 3 (2009) 328 – 336.
[16] R. Clift, J.R. Grace,M.E. Weber, Bubbles, Drops, and Particles, Dover Publications, Mineola, New York, (2005).
[17] L.D. Landau and E.M. Lifshitz. Fluid Mechanics, Pergamon Press, 1987.
[18] V. Bojarevics, G. Djambazov, K. Pericleous. Metall.Materials Trans., 46A (2015) 2884 – 2892.
[19] N. El-Kaddah, T. S. Piwonka and J. T. Berry, US Patent Number 5033948, 1991.

Acknowledgment

The authors acknowledge financial support from the ExoMet Project (co-funded by the European Commission (contract FP7-NMP3-LA-2012-280421), by the European Space Agency and by the individual partner organizations). This project has received funding from the European Union's Seventh Framework Programme for research, technological development and demonstration under grant agreement No. 603-718.